ACCOUNTS
of chemical research

# Synergistically Integrated Nanoparticles as Multimodal Probes for Nanobiotechnology

JINWOO CHEON* AND JAE-HYUN LEE
*Department of Chemistry, Yonsei University, Seoul 120-749, Korea*

RECEIVED ON FEBRUARY 12, 2008

**CONSPECTUS**

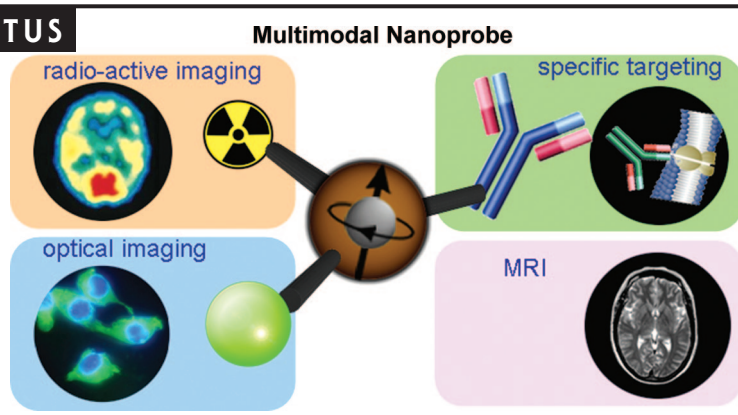


Current biomedical imaging techniques including magnetic resonance imaging (MRI), positron emission tomography (PET), and computed X-ray tomography (CT) are vital in the diagnosis of various diseases. Each imaging modality has its own merits and disadvantages, and a single technique does not possess all the required capabilities for comprehensive imaging. Therefore, multimodal imaging methods are quickly becoming important tools for state-of-the-art biomedical research and clinical diagnostics and therapeutics.

In this Account, we will discuss synergistically integrated nanoparticle probes, which will be an essential tool in multimodal imaging technology. When inorganic nanoparticles are introduced into biological systems, their extremely small size and their exceptional physical and chemical properties make them useful probes for biological diagnostics. Nanoparticle probes can endow imaging techniques with enhanced signal sensitivity, better spatial resolution, and the ability to relay information about biological systems at the molecular and cellular levels.

Simple magnetic nanoparticles function as MRI contrast enhancement probes. These magnetic nanoparticles can then serve as a core platform for the addition of other functional moieties including fluorescence tags, radionuclides, and other biomolecules for multimodal imaging, gene delivery, and cellular trafficking. For example, MRI−optical dual-modal probes composed of a fluorescent dye-doped silica ($DySiO_2$) core surrounded by magnetic nanoparticles can macroscopically detect neuroblastoma cancer cells via MRI along with subcellular information via fluorescence imaging.

Magnetic nanoparticles can also be coupled to radionuclides ($^{124}I$) to construct MRI−PET dual-modal probes. Such probes can accurately detect lymph nodes (LNs), which are critical for assessing cancer metastasis. *In vivo* MRI/PET images can clearly identify small (~3 mm) LNs along with precise anatomical information. Systems using multicomponent nanoparticles modified with biomolecules can also monitor gene expression and other markers in cell therapeutics studies. We have used hybrid stem cell−magnetic nanoparticle probes with MRI to monitor *in vivo* stem cell trafficking. MRI with hybrid probes of magnetic nanoparticles and adenovirus can detect target cells and can monitor gene delivery and the expression of green fluorescent proteins optically. Each component of such multimodal probes complements the other modalities, and their synergistic materials properties ultimately provide more accurate information in *in vitro* and *in vivo* biological systems.

## 1. Introduction

Inorganic nanoparticles possess unique nanoscale size-dependent physical and chemical properties that can be controlled in a manner that is not allowed in bulk size materials.[1] When these tiny materials are introduced into biological systems, their extremely small size and their exceptional


Published on the Web 08/13/2008 www.pubs.acs.org/acr
10.1021/ar800045c CCC: $40.75 

**TABLE 1.** Comparison of Several Imaging Modalities[9]

| imaging technique | source of imaging | spatial resolution | tissue penetrating depth | sensitivity[a] | types of probe |
|---|---|---|---|---|---|
| magnetic resonance imaging (MRI) | radiowave | 25−100 $\mu$m | no limit | mM to $\mu$M (low) | para- ($Gd^{3+}$) or superparamagnetic ($Fe_3O_4$,) materials |
| positron emission tomography (PET) | $\gamma$-ray | 1−2 mm | no limit | pM (high) | radionuclides ($^{18}F$, $^{11}C$, $^{13}N$, $^{15}O$, $^{124}I$, $^{64}Cu$) |
| computed tomography (CT) | X-ray | 50−200 $\mu$m | no limit | not well characterized | high atomic number atoms (iodine, barium sulfate) |
| optical fluorescence imaging | visible or near-infrared light | *in vivo*, 2−3 mm; *in vitro*, sub-$\mu$m | <1 cm | nM to pM (medium) | fluorescent dyes, quantum dots |

[a] Sensitivity of detecting probe is relative to background.

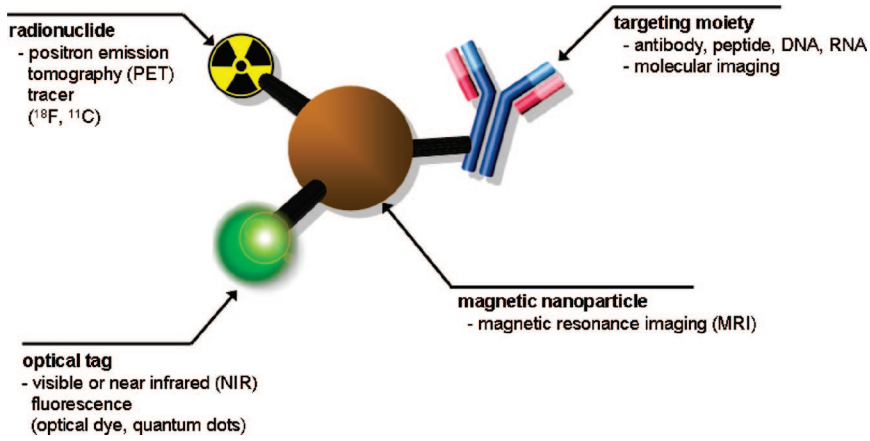


**FIGURE 1.** A schematic of a multimodal imaging probe. A magnetic nanoparticle, radionuclide, optical tag, and targeting moiety are integrated into a single system, which acts as a multimodal molecular imaging platform.

nanoscale materials properties enable them to be useful as probes and delivery vectors for next-generation biological diagnostics and therapeutics. Such new materials and tools developed from nanotechnology are increasingly important for the advancement of several techniques in the biomedical sciences. In particular, biomedical imaging research has been one of the most successful interdisciplinary fields. During the past few years, research in the biomedical fields has exploded and has shown that the potential exists for making what were once thought to be extravagant ideas into reality.[2−7] For example, metallic gold nanoparticles with surface plasmon behavior have been used as unique optical probes for colorimetric sensing and ultrasensitive surface-enhanced Raman detection of biomolecules such as DNA and cancer markers.[2] Semiconducting quantum dots have been used as probes for optically imaging many biological systems ranging from DNA, small organelles, and tumors to biological activities including cell to cell interactions and cell signaling processes.[3] Magnetic nanoparticles have been utilized for magnetic field driven drug delivery and separation, cellular magnetotransduction signaling, hyperthermia and MRI contrast agents.[4−7] However, despite such remarkable progresses in the utilization of nanoparticles for applications in the biomedical sciences, most of the currently developed nanoparticle probes are limited to a single imaging modality.

Target specificity, noninvasiveness, high spatial resolution, 3-D tomography, and real-time imaging are some of the important requirements for next-generation biomedical technologies in which accurate and real-time imaging of biological targets is essential not only to understand the fundamental biological processes but also to successfully diagnose various diseases.[8] However, a single imaging modality alone does not possess the necessary capabilities to do this (Table 1).[9] For example, MRI and CT have the advantages of being noninvasive techniques for *in vivo* imaging and three-dimensional tomography, but they are limited by low target sensitivity. On the other hand, radioactive imaging techniques such as PET have very high target sensitivity but poor spatial resolution. Other optical imaging methods such as fluorescence have relatively good sensitivity but suffer from low tissue penetration depths. In short, each imaging modality has its own merits and disadvantages, but by combination of different modalities into a single system, multimodal imaging methods can compensate for the deficiencies of single imaging modalities. Due to these combined advantages, nanoparticle probes with multimodalities are becoming important tools for

biomedical applications and clinics. A variety of combinations of different modalities including MRI−optical, PET−near-infrared optical fluorescence (NIRF), and PET−CT are possible.[10]

Conventional imaging techniques typically provide anatomical and physiological information at most but have difficulty providing precise information of biological systems at the molecular level. Therefore, essential players in next-generation biomedical techniques are nanoparticle-based multimodal imaging probes, which not only enhance imaging sensitivity and resolution but also possess specificity for so-called "molecular imaging" capabilities. One of the advantages of nanoparticle probes is their flexibility when conjugated with a variety of molecular moieties such as DNAs, peptides, and antibodies for monitoring specific molecular events (e.g., gene expression) and other biological processes (e.g., cell metastasis).

Currently, some prototypes of multimodal nanoparticle probes have been introduced. For instance, MRI−optical probes in which magnetic nanoparticles are fused with optical dyes or fluorescent quantum dots have been demonstrated.[11] Especially for cases in which near-infrared fluorescence (NIRF) dyes are used, enhanced tissue penetration along with MR imaging makes *in vivo* tumor detection possible.[11a] Other types of MRI−optical probes can be magnetic component doped quantum dots and paramagnetic $Gd^{3+}$ chelates with fluorescent dyes.[12] Radionuclide−optical or −MR imaging probes have also been developed in which $\gamma$-ray radionuclides are conjugated with either paramagnetic agents or optical fluorescence dyes.[13] *In vivo* animal organ biodistribution can be clearly monitored when such dual-modal probes are utilized for NIRF−single photon emission computed tomography (SPECT) imaging. Despite such successful results, the development of multimodal nanoparticle probes is still in the early stages.

In this Account, we will briefly discuss the basic concepts of MRI and the key issues (size, composition, and single vs aggregated nanoparticle states) in the design of state-of-the-art magnetic nanoparticle probes with high MR signal sensitivity. Based on the use of magnetic nanoparticles as the core material, more functionalities such as radionuclides, optical tags, targeting moieties, and drugs or gene carriers can be added to construct multimodal nanoparticle probes (Figure 1). Their unique utilizations in multimodal imaging techniques including MRI−optical and MRI−PET of various biological targets and processes such as cancer identification, cancer metastasis, gene delivery, and cell trafficking will be discussed.

## 2. Basics of MRI and Its Relationship to Magnetic Nanoparticles

MRI provides three-dimensional tomographic images by measuring proton relaxation processes of water in biological systems. Under a given external magnetic field ($\mathbf{B}_0$), a small portion of the proton nuclei aligns in the $\mathbf{B}_0$ direction, and the aligned nuclei start to gyroscopically precess with a net magnetic moment of $m$ and a Larmor precession frequency of $\omega_0 = \gamma\mathbf{B}_0$ ($\gamma = 2.67 \times 10^8$ rad·s$^{-1}$·T$^{-1}$ for $^1$H). When a resonant radio frequency (RF) transverse pulse is perpendicularly applied to $\mathbf{B}_0$, it causes resonant excitation of the magnetic moment precession into the perpendicular plane. Upon removal of the RF, the magnetic moment gradually relaxes to equilibrium by realigning to $\mathbf{B}_0$. Such relaxation processes involve two pathways: longitudinal relaxation accompanying loss of energy from the excited state to its surroundings (lattice) and transverse relaxation from the loss of phase coherence of the precessing nuclei spins in the $xy$ plane due to spin−spin interaction (Figure 2a−c). These processes can be expressed as follows.[14]

$$m_z = m(1 - e^{-t/T1}) \qquad \text{(longitudinal)} \qquad (1a)$$

and

$$m_{xy} = m \sin(\omega_0 t + \phi)e^{-t/T2} \qquad \text{(transverse)} \qquad (1b)$$

where $T1$ and $T2$ are the longitudinal and transverse relaxation time, respectively.

MRI records such relaxation processes and then reconstructs them to obtain 3-D gray scale images. Areas with faster $T1$ relaxation are imaged as whiter contrast in $T1$-weighted MRI, while areas with faster $T2$ relaxation are imaged as darker contrast in $T2$-weighted MRI. Biological tissues and organs have aqueous environments that vary in density and homogeneity, which are imaged as different contrast and provide anatomical information. In some cases, however, the contrast difference between tissues (e.g., normal vs cancer) is subtle and is unable to provide precise imaging information. Furthermore, MRI alone provides anatomical information but does not give molecular/biological information on the region of interest.

The role of magnetic nanoparticle probes is not only to enhance contrast differences in biological targets from other tissues but also to provide molecular imaging capabilities. Under a magnetic field of $\mathbf{B}_0$, nanoparticles are magnetized with a moment of $\mu$, and an induced magnetic field establishes a substantial local perturbing dipolar field in its surroundings. Such local magnetic field inhomogeneities accelerate the dephasing rate of the Lamor precession of sur-

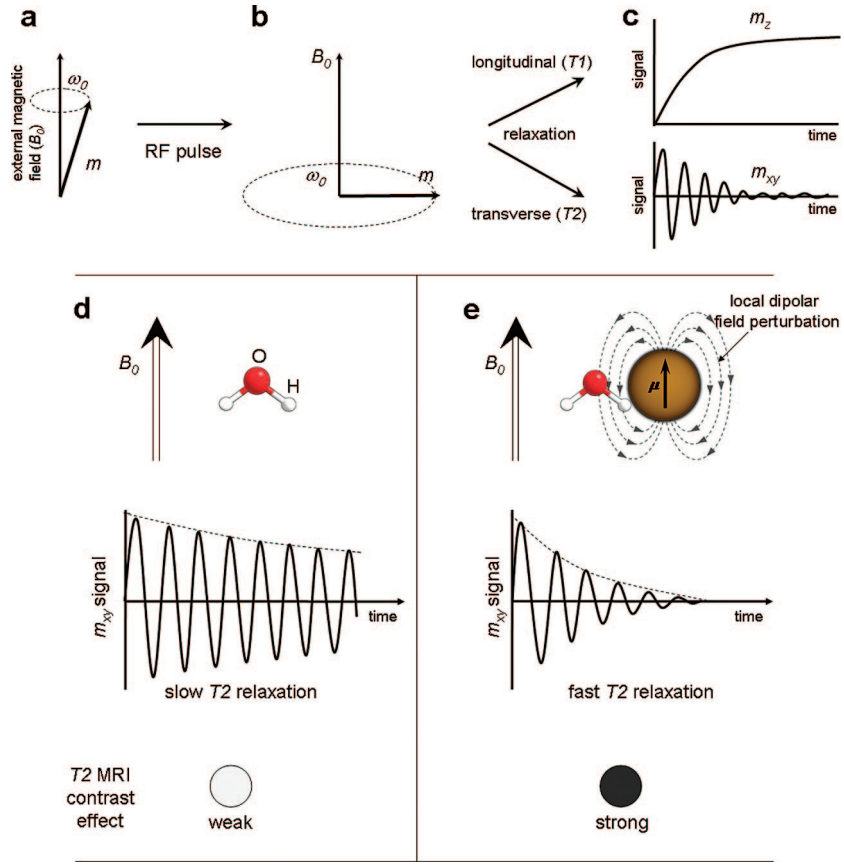


**FIGURE 2.** Illustration of the magnetic resonance (MR) principle and the role of magnetic nanoparticles as a contrast agent: (a) net magnetic spins ($m$) of water protons precess with a Larmor frequency ($\omega_0$); (b) upon application of a RF pulse, $m$ begins precessing perpendicular to $\mathbf{B}_0$; (c) $m$ relaxes back to its original equilibrium states through longitudinal ($T1$, $m_z$) and transverse in-planar ($T2$, $m_{xy}$) modes; (d) for in-planar ($T2$) relaxation mode without magnetic nanoparticle, water protons have a relatively slow relaxation time with a weak MR contrast effect; (e) in the presence of magnetic nanoparticles, protons inside the local dipolar field perturbation area around the nanoparticle relax faster with a strong MRI signal, which produces strong MR contrast effects.

rounding water molecules with a reduction of $T2$ (Figure 2d,e). According to the outer sphere spin−spin relaxation approximation, the relaxivity $R2$ (=1/$T2$) of the nanoparticle containing water solution is expressed as[15]

$$R2 = \frac{1}{T2} = \left(\frac{32\pi}{405}\right)\gamma_I^2\mu^2\frac{N_A}{1000}\left(\frac{[M]}{rD}\right)\{6.5j_2(\omega_S) + 1.5j_1(\omega_I) + 2j_1(0)\} \quad (2)$$

where M = molarity of the magnetic nanoparticle, $r$ = nanoparticle radius; $j_n(\omega,\tau)$ = spectral density function; $\mu$ = transverse component of magnetic moment of nanoparticle; $\gamma_I$ = gyromagnetic ratio of protons; $N_A$ = Avogadro's number, and $\omega_S$ and $\omega_I$ = Larmor angular precession frequency of the nanoparticle and water proton magnetic moments, respectively.

According to eq 2, the spin−spin relaxation time ($T2$) is inversely proportional to the square of the magnetic moment ($\mu$) of the particle. In the nanoscale regime, these values can be precisely tuned by controlling nanoparticle characteristics

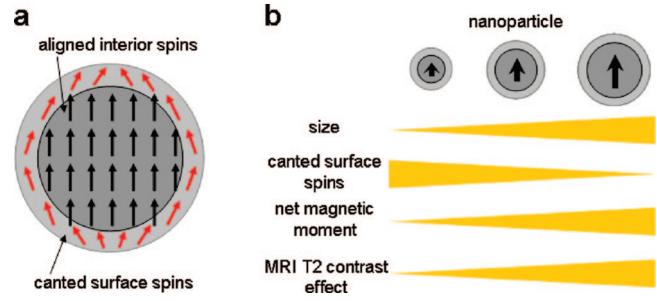


**FIGURE 3.** Nanoparticle size effects on magnetism and MR contrast enhancement: (a) canted surface atoms surrounding core magnetic atoms; (b) surface to volume ratio vs size, canted surface spins, net magnetic moment, and $T2$ contrast effect.

such as size, shape, composition, and crystallinity.[6,16−19] For example, smaller nanoparticles with higher surface to volume ratios possess a weaker net magnetic moment caused by the large contribution of canted magnetic spin states on the surface (Figure 3). Such size effects have been experimentally demonstrated in the case of $Fe_3O_4$-based magnetism engineered iron oxide (MEIO) nanoparticles.[6a] The mass magne-

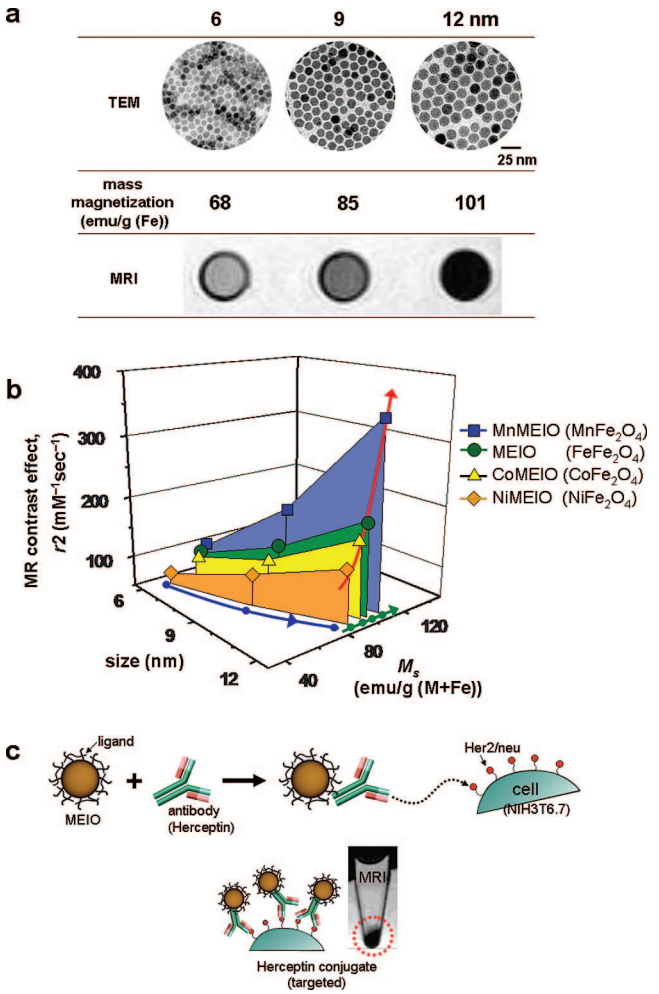


**FIGURE 4.** Magnetic nanoparticle size and dopant effects on mass magnetization ($M_s$) and MRI contrast enhancement ($r2$): (a) size effect of the MEIO (magnetism engineered iron oxide) nanoparticles; (b) overall relationship graphs of nanoparticle size, dopants, magnetization ($M_s$), and $T2$ MRI contrast ($r2$) for M-MEIO (M = Mn, Fe, Co, Ni)—size effect on $M_s$ (blue arrow), composition effect on $M_s$ (green arrows), and composition effect on $T2$ MRI contrast ($r2$) (red arrow); (c) Herceptin, (antibody against the Her2/neu cancer marker) conjugated MEIO nanoparticle probes specifically detect cancer cells (dark MR contrast) with high sensitivity. Reproduced with permission from ref 6b. Copyright 2005 American Chemical Society.

tization value ($M_s$) increases from 68 to 85 and 101 emu/g (Fe) as the MEIO size increases from 6 to 9 and 12 nm, respectively (Figure 4a). Similar size effects are shown for metal ferrites with different compositions ($MFe_2O_4$, M = Mn, Co, Ni) (Figure 4b, blue arrow). The mass magnetization value can be further tuned by introducing chemical dopants with different magnetic spins into the host MEIO nanoparticles. For example, the replacement of octahedral $Fe^{2+}$ in 12 nm MEIO with other magnetic metal dopants such as $Mn^{2+}$, $Co^{2+}$, and $Ni^{2+}$ results in the systematic change in their $M_s$ to 110, 99, and 85 emu/g, respectively (Figure 4b, green arrow).[19] Higher mass magnetization of the nanoparticle results in stronger MR contrast effects with larger $R2$ relaxivity coefficient value ($r2$). For 12 nm M-MEIO, the $r2$ increases from 152 to 172, 218, and 358 $mM^{-1}$ $s^{-1}$ for M = Ni, Co, Fe, and Mn, respectively (Figure 4b, red arrow). With such strong MR contrast effects, upon being chemically conjugated with a cancer targeting moiety such as Herceptin antibody, 12 nm MEIO probes can specifically detect small size cancer with high sensitivity (Figure 4c).[19]

When nanoparticles are brought into proximity, they start to communicate with each other, which leads to changes in their properties. If magnetic nanoparticles are close together and make agglomerates, magnetic spin moments are coupled to generate stronger magnetic fields (Figure 5a).[20] The magnetic coupling effect, which directly influences the MR contrast and the $R2$ relaxivity, is expressed as[21]

$$R2 = \frac{1}{T2} = \left(\frac{64\pi}{135}\right)\left(\mu N_g \frac{L(x)}{4\pi}\right)^2 \frac{N_A C_a}{R_a D} \qquad (3)$$

where $\mu$ = magnetic moment of the nanoparticle, $N_g$ = number of nanoparticles in an agglomerate, $C_a$ = concentration of agglomerates, $R_a$ = radius of an agglomerate, $D$ = water diffusion coefficient, $N_A$ = Avogadro's number, and $L(x)$ = Langevin function. According to this equation, $R2$ is proportional to $\mu$ and $N_g$.

Utilization of magnetic coupling effects of nanoparticles enables highly sensitive magnetic resonance sensing of various biological targets in which the MR signal changes according to the degree of dispersed and assembled states of biological targets. For example, detection of biological assembling events such as amyloid $\beta$ (A$\beta$) fibril formation, which is a key process for Alzheimer's disease, is possible. The plaque formation of A$\beta$ involves progressive stages: from monomer to oligomers, to protofibrils, and to fibril stages.[22] A highly sensitive MRI probe such as Co@Pt–Au heterodimer nanoparticle comprised of a Co@Pt core–shell particle having roughly three times stronger magnetization than iron oxide nanoparticles and Au which is useful for relatively facile bioconjugation. Figure 5b depicts the schematic of A$\beta$ sensing in which the neutravidin (NTV) conjugated Co@Pt–Au nanoparticle probe binds to the biotinylated A$\beta$. At each different stage of the A$\beta$ assembly process, the number of nanoparticles attached to the A$\beta$ assembly changes and finally leads to an MRI signal change at each successive stage (Figure 5c,d). MRI response is very sensitive at the early protofibril stage with a large change in $\Delta T2$.[23] This study indicates that this particular nanoparticle probe is useful for the MRI of dynamic assem-

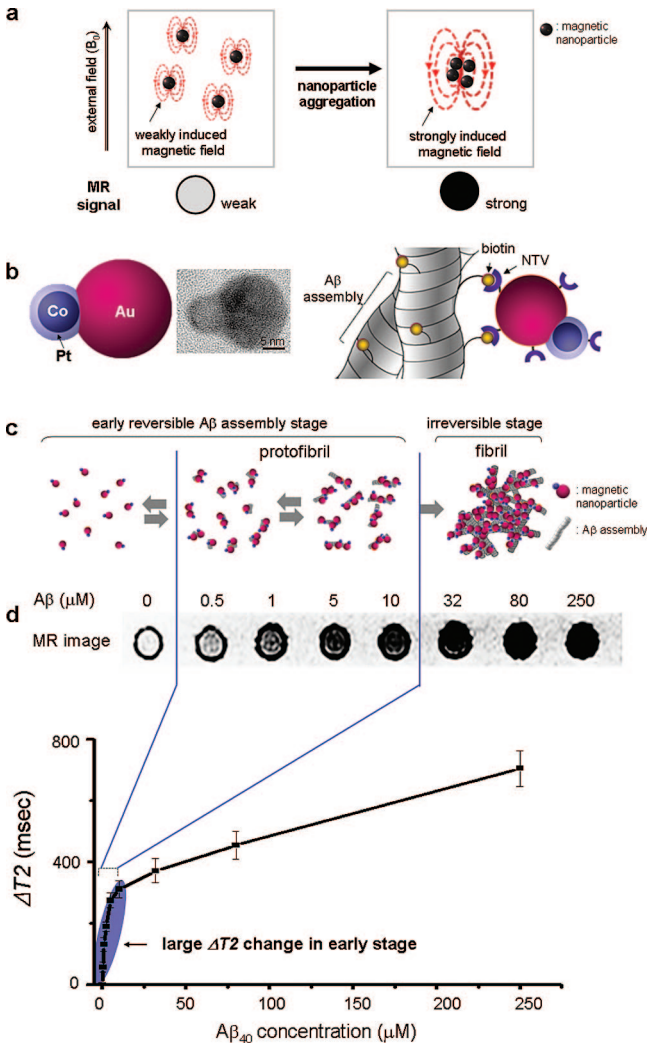


**FIGURE 5.** Magnetic nanoparticle aggregation effects on the sensing of amyloid $\beta$ (A$\beta$) peptides via MRI: (a) MR signal change for free standing magnetic nanoparticles vs aggregated nanoparticles; (b) a schematic of the Co@Pt–Au nanoparticle with a TEM image—NTV coated Co@Pt–Au selectively binds to the biotinylated A$\beta$ peptide; (c) concentration-dependent A$\beta$ formation—NTV-Co@Pt–Au nanoparticles are used as MR probes; (d) A$\beta$ assembly stage dependent MRI—larger contrast change ($\Delta T2$) is observed in the early reversible protofibril formation stages. Reproduced with permission from ref 23. Copyright 2008 Royal Society of Chemistry.

bly processes of A$\beta$ protofibrils and has the potential to diagnose the early stages of Alzheimer's disease.

## 3. Synergistic Effects of Integrated Nanoparticle Probes for Multimodal Imaging and Reporting Capabilities

As described previously, it is clear that structures containing multiple imaging modalities combined with MRI have merit for potentially false-free sensing and imaging of various biological targets and processes with high sensitivity and specificity.

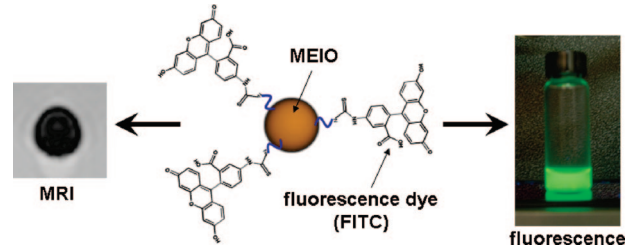


**FIGURE 6.** MRI–optical dual-modal probes consisting of 12 nm MEIO nanoparticles and FITC fluorescent dye molecules with a dark MRI contrast effect and optical signal.

For multimodal probe fabrication, the integration of multicomponents into a nanoparticle is required. Such nanoparticle probes can be easily fabricated via chemical conjugations by using a variety of cross-linker molecules. In addition, epitaxial growth is another method for fabricating core–shell or heterodimer structured inorganic nanoparticles, where a secondary component is epitaxially grown on the primary nanoparticle.[24]

The significant impact of such multimodal probes can also be realized in the fact that they can provide molecular information (e.g., biomarkers, gene expression), biological processes (e.g., metastasis, cell trafficking), and anatomical information. One of the well-studied examples is the MRI–optical dual-modal nanoparticle probes in which magnetic nanoparticles are chemically conjugated with fluorophores.[11] Figure 6 shows a MRI–optical dual-modal probe in which FITC (fluorescein isothiocyanate) dyes are directly conjugated to a 12 nm MEIO nanoparticles via chemical reactions between isothiocyanate on FITC and amine on MEIO. Although this type of probe works reasonably nicely, there is the potential adversity including photobleaching and rapid fluorescence quenching effects.

As a more robust and advanced MRI–optical probe, core–satellite nanoparticle probes comprised of a fluorescent dye-doped silica ($DySiO_2$) core nanoparticle and multiple surrounding magnetic nanoparticles are proposed. Two nanoparticles are linked through a Michael addition reaction between the thiol groups on MEIO nanoparticles and the maleimide groups on $DySiO_2$ nanoparticles (Figure 7a). Such hybrid core–satellite structures are advantageous because they provide a more stable optical signal owing to the dye protection that is provided inside the porous silica structure. Enhanced MR signals also result due to magnetic coupling between MEIO nanoparticles. Hybrid nanoparticles exhibit 1.7 times higher fluorescence intensity at 580 nm compared with fluorescent dyes such as rhodamine that are directly attached to MEIO nanoparticles. More importantly, they also have an $r2$ value of 397 $mM^{-1}$ $s^{-1}$, which is 3.4 times higher than that

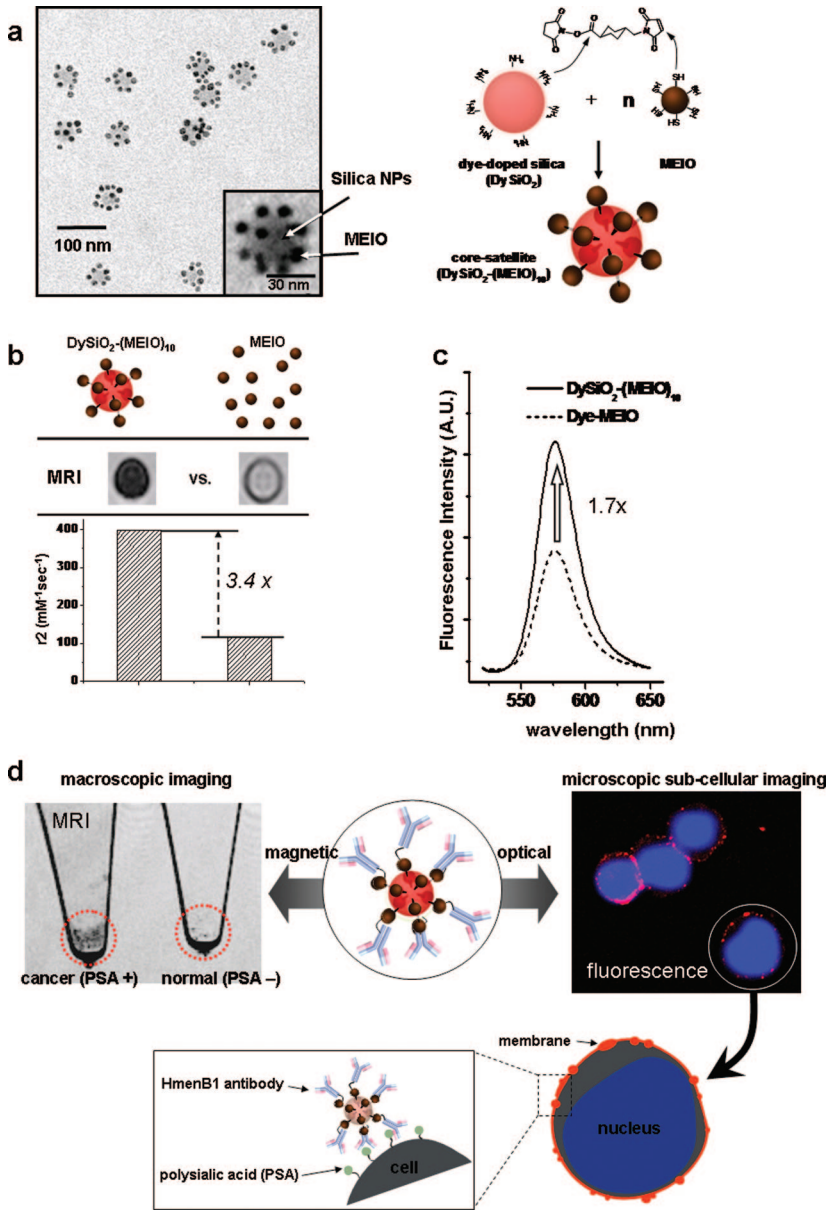


**FIGURE 7.** $DySiO_2-(MEIO)_{10}$ for dual-modal MRI–optical imaging: (a) TEM and schematic diagram for the synthesis of $DySiO_2-(MEIO)_{10}$; (b) synergistic MR contrast enhancement effect of $DySiO_2-(MEIO)_{10}$ ($r2 = 397\ mM^{-1}\ s^{-1}$) with a 3.4 times higher value compared with free MEIO nanoparticles; (c) 1.7 times higher fluorescent intensity is observed for $DySiO_2-(MEIO)_{10}$; (d) HmenB1 antibody conjugated $DySiO_2-(MEIO)_{10}$ selectively detects neuroblastoma cancer cells with PSA receptors. Reproduced with permission from ref 26. Copyright 2006 Wiley-VCH.

of free MEIO nanoparticles (Figure 7b,c). The nanoparticle probes are further conjugated with HmenB1 antibody, which specifically recognizes a cancer marker such as polysialic acids (PSA) for the imaging of neuroblastoma cancer cells.[25] The hybrid nanoparticles successfully target only CHP-134 neuroblastoma cells marked with the PSAs as indicated by the areas of dark MR contrast (Figure 7d). Such MRI provides a rather macroscopic image with a ~50 $\mu$m spatial resolution. On the other hand, *in vitro* fluorescent imaging can exhibit detailed microscopic information at the subcellular level. Confocal microscope imaging shows intense red fluorescence only in the cell membrane region without any signals from the nuclei and cytosol regions, indicating that the PSA biomarkers are distributed only on the membrane surface (Figure 7d).[26]

Magnetic nanoparticles can also be coupled with radionuclide labels for dual-mode MRI–radionuclide imaging using a gamma camera and PET. These two radioactive imaging techniques use the intense $\gamma$-ray emission from radionuclides for much higher sensitivity than other imaging methods such MRI and CT. Figure 8 is a typical gamma camera SPECT image of a mouse in which the magnetic MEIO–$^{111}$In nanoparticle probe is injected via the tail vein for the detection of tumors

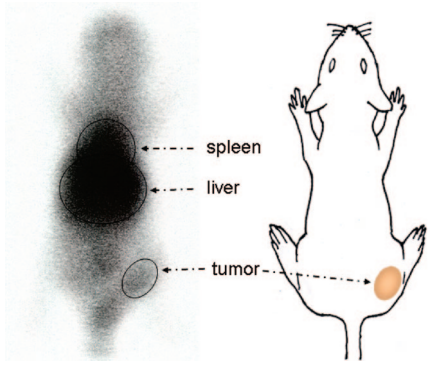


**FIGURE 8.** SPECT image of a mouse in which the $^{111}$In–MEIO nanoparticles are injected via the tail vein.

and other organs. As seen, the targeted regions in the SPECT images are poorly defined in terms of spatial resolution and a clear distinction among different organs is difficult.

MRI–PET has the potential for providing better spatial resolution with anatomical information and also improved signal sensitivity. PET uses positrons to create $\gamma$-rays and provides more accurate spatial information with roughly 15 times higher signal sensitivity than SPECT. The use of $^{124}$I-labeled MnMEIO dual-modal nanoparticles for *in vivo* detection of the sentinel lymph node (LN) is a good example. The lymphatic system is a first biological defense system against infection, but it is also used as a passage in the metastasis of cancer.[27] For this reason, accurate imaging and characterization of LNs are critical for the diagnosis and treatment of cancer. $^{124}$I is directly conjugated to the innate tyrosine residue of serum albumins, which are coated onto the MnMEIO magnetic nanoparticles. When $^{124}$I-labeled MnMEIO nanoparticles are injected into the forepaw of a mouse, small sized (~3 mm) brachial LNs located deep inside the body are clearly imaged. Figure 9b–d shows PET, MR, and PET/MR fusion images of a rat. PET alone gives a very intense red signal from LNs but without any anatomical information. MR provides a nice anatomical image of the upper body of the rat along with a couple of dark spots identified as potential LNs. Only when these two images are overlaid is clear identification of a brachial LN possible. The impact of dual PET/MR probes is high especially for *in vivo* applications since PET provides extremely high signal sensitivity and MRI merits from precise anatomical information in addition to their noninvasive 3-D tomographic capabilities.[28]

The usability of multicomponent magnetic nanoparticle probes is not limited to diagnostic purposes but can be extended to the monitoring of therapeutic and gene expression studies. Upon hybridization with biologically active species such as stem cells and viruses, they can play a role as probes for biological processes such as cell trafficking and gene delivery under *in vitro* and *in vivo* conditions.[29,30]

Hybrid stem cell–magnetic nanoparticles can be used as dual-function probes possessing both *in vivo* MRI trafficking and stem cell functions, which are thought to have the potential to revolutionize current therapeutics since they have specific targeting and tissue regeneration capabilities.[31] After MEIO nanoparticles are transfected into the neural stem cells via electrostatic interactions, the neural stem cell–MEIO nanoprobes are injected into an injured rat

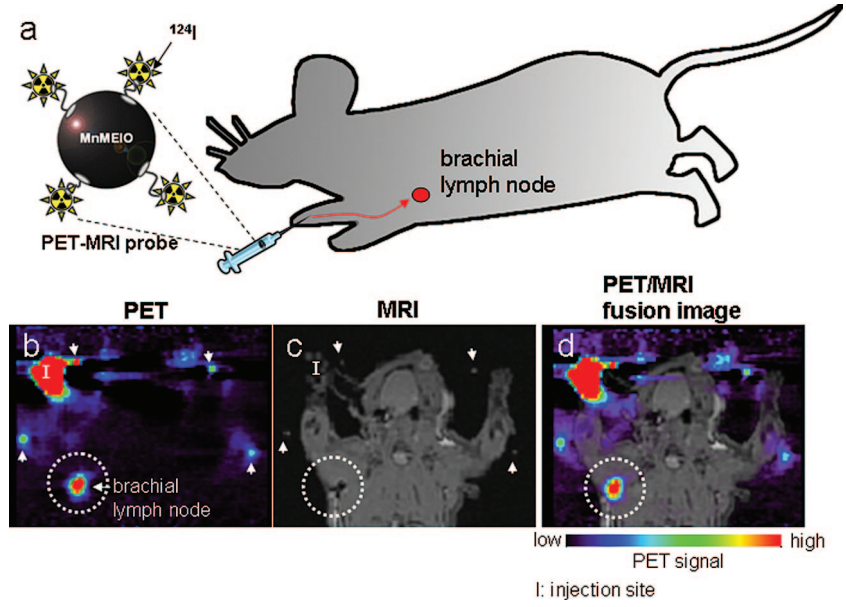


**FIGURE 9.** *In vivo* MRI–PET dual-modal imaging: (a) MnMEIO–$^{124}$I conjugate probes are injected into the forepaw of a rat for the detection of lymph node; (b) PET image; (c) MR image; (d) PET/MR fusion image. The white circle denotes the location of a brachial lymph node. Reproduced with permission from ref 28. Copyright 2008 Wiley-VCH.

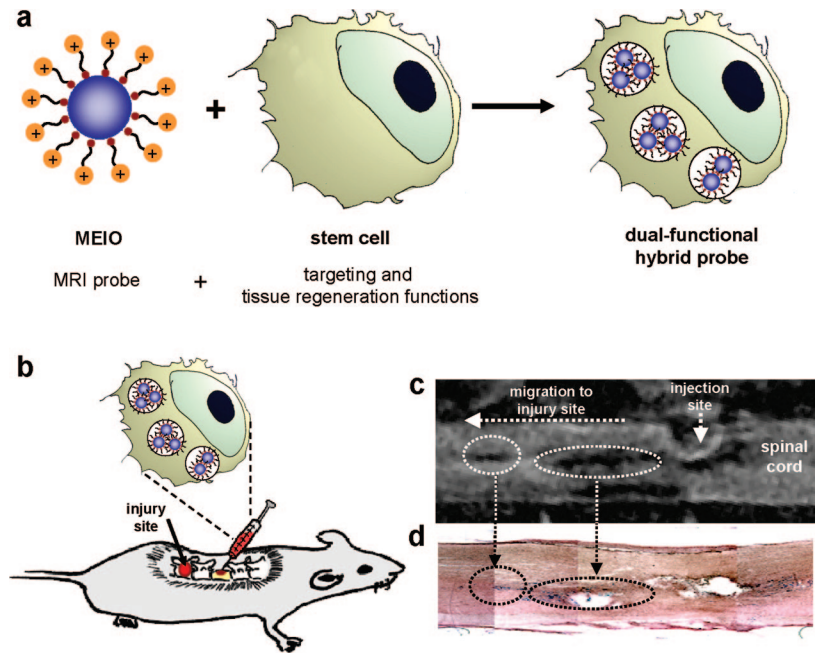


**FIGURE 10.** MEIO−stem cell hybrid probes possessing dual functionality of MEIO (MRI) and stem cell (targeting and tissue regeneration): (a) MEIO nanoparticles are transfected into the neural stem cells via electrostatic interactions; (b) MEIO−stem cell hybrid probes are injected into a rat with an injured spinal cord; (c) *in vivo* MRI of a rat spinal cord three weeks after the injection—elongated dark MR contrasts along the spinal cord are observed; (d) *ex vivo* histological image of the spinal cord stained by Prussian blue matches with the MR image. Reproduced with permission from ref 29. Copyright 2005 American Chemical Society.

spinal cord (Figure 10b). MR images taken after three weeks reveal that injected nanoprobes slowly migrate toward the injury site, which is imaged as two elongated dark MR signals (Figure 10c). *Ex vivo* histological examination by Prussian blue staining, which detects the iron oxides, confirms that the stained regions are reasonably well-matched with those characterized by MRI (Figure 10c,d).[29] This result indicates that stem cell−MEIO hybrid nanoparticles are indeed effective probes for cellular trafficking and can be useful for long-term monitoring of stem cell based tissue regeneration processes and therapeutics.

As another example, hybrid nanoparticle probes composed of magnetic nanoparticles and an adenovirus are useful for simultaneous MR imaging and gene delivery purposes. Adenoviral gene delivery is known to be ~8000 times more effective than other gene delivery vectors along with target specificity to the cells with CAR (Coxsackie adenovirus receptor).[32,33] Such hybrid nanoparticles are fabricated by cross-linking between a maleimide-modified adenovirus and thiol-functionalized MnMEIO nanoparticles resulting in an adenovirus core with an enhanced green fluorescent protein (eGFP) promoter gene and multiple MnMEIO satellite nanoparticles (Figure 11a). *In vitro* MR imaging of the hybrid nanoparticle treated cells shows dark MR signals specifically from the CAR positive U251N cells whereas no MR contrast is observed from the control cells. Such MR results are consistently correlated to successful eGFP gene delivery in which intense green fluorescence is only observed from the CAR positive cells (Figure 11c).[30] As seen in TEM analyses (Figure 11d), adenovirus−MnMEIO nanoparticle probes possibly go through the endocytosis process and form multiple endosomes (solid circles). Some probes are also observed in the proximity of the nucleus (dashed circles). The significance of this study is that hybrid probes possess the capabilities of targeted infection, MR imaging, and gene expression simultaneously and have the potential for *in vivo* MR tracking for gene based therapies of target diseases.

## 4. Conclusions

As discussed in this Account, by integrating anatomical and molecular based imaging capabilities, multimodal nanoparticle probes are becoming important in the paradigm shift from conventional to future imaging technologies, which will provide critical molecular and cellular level information not only for false-free diagnostics and advanced therapeutics but also toward the better understanding of fundamental biological processes. Such multimodal probes can be easily extended to therapeutic applications by simply adding drug molecules into the probes or by using the magnetic compo-

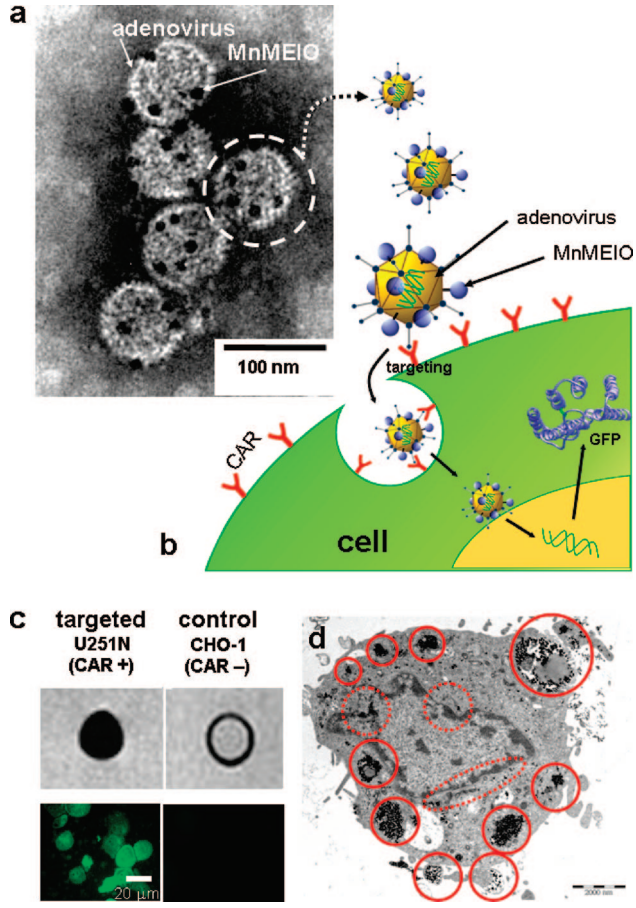


**FIGURE 11.** Adenovirus–MnMEIO hybrid nanoparticle probes for targeted MR imaging and gene delivery: (a) TEM image of the adenovirus–MnMEIO hybrid nanoparticles; (b) a schematic of the targeting and gene delivery processes using the adenovirus–MnMEIO hybrid nanoparticle probes, which are internalized through CAR-mediated endocytosis processes; (c) such events are imaged only in the CAR-positive cells by a dark contrast in MRI and the vivid GFP (green fluorescent protein) gene expression; (d) TEM image of adenovirus–MnMEIO hybrid nanoprobe treated U251N cells. Solid circles indicate nanoprobes either under endocytosis or trapped inside endosomes. Dashed circles indicate some nanoprobes found near the nuclear membrane. Reproduced with permission from ref 30. Copyright 2007 Wiley-VCH.

nent as a heat generator for hyperthermia or as a guiding vector to the targeted area.[34] Although still in its early stages with only a handful of successfully demonstrated cases, the continued development of such multimodal probes is increasingly important for advancing this exciting and rapidly changing research field.

*We acknowledge Dr. Young-wook Jun for his helpful discussion. This research is supported by the National Research Laboratory (Grant M10600000255), Nano-Bio Science & Technology Program (Grant M1050300218-05M0300-21810), AOARD-AFOSR, NCI Center for Cancer Nanotechnology Excellence (CCNE), NBIT (Grant K20716000001-07A0400-00110), and 2nd stage BK21 for Chemistry.*

## BIOGRAPHICAL INFORMATION

**Jinwoo Cheon** is a chemistry professor of Yonsei University, the director of Convergence Nanomaterials National Research Laboratory, and the head of the Nanomaterials Division of the Nano-Medical National Core Research Center of Korea. He graduated from Yonsei University with B.S. and received his Ph.D. from University of Illinois, Urbana–Champaign, in 1993. After postdoctoral training at U.C. Berkeley and also at UCLA, he joined KAIST as an assistant professor. In 2002, he moved to Yonsei University. His current research interest includes the development of functional inorganic nanostructures and their applications for biomedical and energy related sciences.

**Jae-Hyun Lee**, born in Seoul, Korea, graduated from Yonsei University in 2003 with his B.S. He is a graduate student pursuing his Ph.D. in chemistry under the supervision of Professor Jinwoo Cheon. His current research interests are the fabrication of bioactivatable hybrid magnetic nanoparticles for molecular imaging and therapeutics. He is a recipient of the Korea Research Foundation Fellowship (2004), Seoul Science Fellowship (2005), and Yonsei Graduate Student Research Award (2007).

## FOOTNOTES

*To whom correspondence should be addressed. E-mail: jcheon@yonsei.ac.kr.

## REFERENCES

1 (a) Alivisatos, A. P. Semiconductor Clusters, Nanocrystals, and Quantum Dots. *Science* **1996**, *271*, 933–937. (b) Murray, C. B.; Norris, D. J.; Bawendi, M. G. Synthesis and Characterization of Nearly Monodisperse CdE (E = sulfur, selenium, tellurium) Semiconductor Nanocrystallites. *J. Am. Chem. Soc.* **1993**, *115*, 8706–8715. (c) Link, S.; El-Sayed, M. A. Spectral Properties and Relaxation Dynamics of Surface Plasmon Electronic Oscillations in Gold and Silver Nanodots and Nanorods. *J. Phys. Chem. B.* **1999**, *103*, 8410–8426.

2 (a) Cao, Y. W.; Jin, R.; Mirkin, C. A. Nanoparticles with Raman Spectroscopic Fingerprints for DNA and RNA Detection. *Science* **2002**, *297*, 1536–1540. (b) Elghanian, R.; Storhoff, J. J.; Mucic, R. C.; Letsinger, R. L.; Mirkin, C. A. Selective Colorimetric Detection of Polynucleotides Based on the Distance-Dependent Optical Properties of Gold Nanoparticles. *Science* **1997**, *277*, 1078–1081. (c) Qian, X.; Peng, X.-H.; Ansari, D. O.; Yin-Goen, O.; Chen, G. Z.; Shin, D. M.; Yang, L.; Young, A. N.; Wang, M. D.; Nie, S. In Vivo Tumor Targeting and Spectroscopic Detection with Surface-Enhanced Raman Nanoparticle Tags. *Nat. Biotechnol.* **2007**, *26*, 83–90.

3 (a) Michalet, X.; Pinaud, F. F.; Bentoilla, L. A.; Tsay, J. M.; Doose, S.; Li, J. J.; Sundaresan, G.; Wu, A. M.; Gambhir, S. S.; Weiss, S. Quantum Dots for Live Cells, in Vivo Imaging, and Diagnostics. *Science* **2005**, *307*, 538–544. (b) Medintz, I. L.; Uyeda, H. T.; Goldman, E. R.; Mattoussi, H. Quantum Dot Bioconjugates for Imaging, Labelling and Sensing. *Nat. Mater.* **2005**, *4*, 435–446. (c) Kim, S.; Lim, Y. T.; Soltesz, E. G.; De Grand, A. M.; Lee, J.; Nakayama, A.; Parker, J. A.; Mihaljevic, T.; Laurence, R. G.; Dor, D. M.; Cohn, L. H.; Bawendi, M. G.; Frangioni, J. V. Near-Infrared Fluoresncet Type II Quantum Dots for Sentinel Lymph Node Mapping. *Nat. Biotechnol.* **2004**, *22*, 93–97.

4 (a) Laurent, S.; Forge, D.; Port, M.; Roch, A.; Robic, C.; Elst, L. V.; Muller, R. N. Magnetic Iron Oxide Nanoparticles: Synthesis, Stabilization, Vectorization, Physicochemical Characterizations, and Biological Applications. *Chem. Rev.* **2008**, *108*, 2064–2110. (b) Jun, Y.-w.; Seo, J.-w.; Cheon, J. Nanoscaling Laws of Magnetic Nanoparticles and Their Applicabilities in Biomedical Sciences. *Acc. Chem. Res.* **2008**, *41*, 179–189. (c) Goodwin, S.; Peterson, C.; Hoh, C.; Bittner, C. Targeting and Retention of Magnetic Targeted Carriers (MTCS) Enhancing Intra-Arterial Chemotherapy. *J. Magn. Magn. Mater.* **1999**, *194*, 132–139. (d) Yavuz, C. T.; Mayo, J. T.; Yu, W. W.; Prakash, A.; Falkner, J. C.; Yean, S.; Cong, L.; Shipley, H. J.; Kan, A.; Tomson, M.; Natelson, D.; Colvin, V. L. Low-Field Magnetic Separation of Monodisperse $Fe_3O_4$ Nanocrystals. *Science* **2006**, *314*, 964–967. (e)

Hahn, Y. K.; Jin, Z.; Kang, J. H.; Oh, E.; Han, M.-K.; Kim, H.-S.; Jang, J.-T.; Lee, J.-H.; Cheon, J.; Kim, S. H.; Park, H.-S.; Park, J.-K. Magnetophoretic Immunoassay of Allergen-Specific IgE in an Enhanced Magnetic Field Gradient. *Anal. Chem.* **2007**, *79*, 2214–2220.

5 (a) Dobson, J. Remote Control of Cellular Behaviour with Magnetic Nanoparticles. *Nat. Nanotech* **2008**, *3*, 139–143. (b) Campbell, R. B. Battling Tumors with Magnetic Nanotherapeutics and Hyperthermia: Turning Up the Heat. *Nanomed.* **2007**, *2*, 649–652. (c) Fortin, J.-P.; Wilhelm, C.; Servais, J.; Ménager, C.; Bacri, J.-C.; Gazeau, F. Size-Sorted Anionic Iron Oxide Nanomagnets as Colloidal Mediators for Magnetic Hyperthermia. *J. Am. Chem. Soc.* **2007**, *129*, 2628–2635.

6 (a) Jun, Y.-w.; Lee, J.-H.; Cheon, J. Chemical Design of Nanoparticle Probes for High-Performance Magnetic Resonance Imaging. *Angew. Chem. Int. Ed.* **2008**, *47*, 5122–5135. (b) Jun, Y.-w.; Huh, Y.-M.; Choi, J.-s.; Lee, J.-H.; Song, H.-T.; Kim, S.-j.; Yoon, S.; Kim, K.-S.; Shin, J.-S.; Suh, J.-S.; Cheon, J. Nanoscale Size Effect of Magnetic Nanocrystals and Their Utilization for Cancer Diagnosis via Magnetic Resonance Imaging. *J. Am. Chem. Soc.* **2005**, *127*, 5732–5733. (c) Seo, W.-S.; Lee, J. H.; Sun, X.; Suzuki, Y.; Mann, D.; Liu, Z.; Terashima, M.; Yang, P. C.; McConnell, M. V.; Nishimura, D. G.; Dai, H. FeCo/Graphitic-Shell Nanocrystals as Advanced Magnetic-Resonance-Imaging and Near-Infrared Agents. *Nat. Mater.* **2006**, *5*, 971–976. (d) Xie, J.; Chen, K.; Lee, H. Y.; Xu, C.; Hsu, A. R.; Peng, S.; Chen, X.; Sun, S. Ultrasmall c(RGDyK)-Coated $Fe_3O_4$ Nanoparticles and Their Specific Targeting to Integrin $\alpha_v\beta_3$-Rich Tumor Cells. *J. Am. Chem. Soc.* **2008**, *130*, 7542–7543. (e) Nasongkla, N.; Bey, E.; Ren, J.; Ai, H.; Khemtong, C.; Guthi, J. S.; Chin, S.-F.; Sherry, A. D.; Boothman, D. A.; Gao, J. Multifunctional Polymeric Micelles as Cancer-Targeted, MRI-Ultrasensitive Drug Delivery Systems. *Nano Lett.* **2006**, *6*, 2427–2430.

7 (a) Weissleder, R.; Moore, A.; Mahmood, U.; Bhorade, R.; Benveniste, H.; Chiocca, E. A.; Basilion, J. P. In Vivo Magnetic Resonance Imaging of Transgene Expression. *Nat. Med.* **2000**, *6*, 351–354. (b) Zhao, M.; Beauregard, D. A.; Loizou, L.; Davletov, B.; Brindle, K. M. Non-Invasive Detection of Apoptosis Using Magnetic Resonance Imaging and a Targeted Contrast Agent. *Nat. Med.* **2001**, *7*, 1241–1244. (c) Artemov, D.; Bhujwalla, Z. M.; Bulte, J. W. Magnetic Resonance Imaging of Cell Surface Receptors Using Targeted Contrast Agents. *Curr. Pharm. Biotechnol.* **2004**, *2*, 165–172. (d) von Maltzahn, G.; Harris, T. J.; Park, J. H.; Min, D. H.; Schmidt, A. J.; Sailor, M. J.; Bhatia, S. N. Nanoparticle Self-Assembly Gated by Logical Proteolytic Triggers. *J. Am. Chem. Soc.* **2006**, *129*, 6064–6065. (e) Liu, W.; Dahnke, H.; Jordan, E. K.; Schaeffter, T.; Frank, J. A. In Vivo MRI Using Positive-Contrast Techniques in Detection of Cells Labeled with Superparamagnetic Iron Oxide Nanoparticles. *NMR Biomed.* **2008**, *21*, 242–250.

8 Weissleder, R. Molecular Imaging in Cancer. *Science* **2006**, *312*, 1168–1171.

9 Massoud, T. F.; Gambhir, S. S. Molecular Imaging in Living Subjects: Seeing Fundamental Biological Processes in a New Light. *Genes Dev.* **2003**, *17*, 545–580.

10 (a) Ntziachristos, V.; Yodh, A. G.; Schnall, M.; Chance, B. Concurrent MRI and Diffuse Optical Tomography of Breast after Indocyanine Green Enhancement. *Proc. Natl. Acad. Sci. U.S.A.* **2000**, *97*, 2767–2722. (b) Beyer, T.; Townsend, D. W.; Brun, T.; Kinahan, P. E.; Charron, M.; Roddy, R.; Jerin, J.; Young, J.; Byars, L.; Nutt, R. A Combined PET/CT Scanner for Clinical Oncology. *J. Nucl. Med.* **2000**, *41*, 1369–1379.

11 (a) Kircher, M. F.; Mahmood, U.; King, R. S.; Weissleder, R.; Josephson, L. A Multimodal Nanoparticle for Preoperative Magnetic Resonance Imaging and Intraoperative Optical Brain Tumor Delineation. *Cancer Res.* **2003**, *63*, 8122–8125. (b) Mulder, W. J. M.; Koole, R.; Brandwijk, R. J.; Storm, G.; Chin, P. T. K.; Strijkers, G. J.; de Mello Donega, C.; Nicolay, K.; Griffioen, A. W. Quantum Dots with a Paramagnetic Coating as a Bimodal Molecular Imaging Probe. *Nano Lett.* **2006**, *6*, 1–6.

12 (a) Wang, S.; Jarrett, B. R.; Kauzlarich, S. M.; Louie, A. Y. Core/Shell Quantum Dots with High Relaxivity and Photoluminescence for Multimodality Imaging. *J. Am. Chem. Soc.* **2007**, *129*, 3848–3856. (b) Hüber, M. M.; Staubli, A. B.; Kustedjo, K.; Gray, M. H. B.; Shih, J.; Fraser, S. E.; Jacobs, R. E.; Meade, T. J. Fluorescently Detectable Magnetic Resonance Imaging Agents. *Bioconjugate Chem.* **1998**, *9*, 242–249.

13 (a) Zhang, Z.; Liang, K.; Bloch, S.; Berezin, M.; Achilefu, S. Monomolecular Multimodal Fluorescence-Radioisotope Imaging Agents. *Bioconjugate Chem.* **2005**, *16*, 1232–1239. (b) Zielhuis, S. W.; Seppenwoolde, J.-H.; Mateus, V. A. P.; Bakker, C. J. G.; Krijger, G. C.; Storm, G.; Zonnenberg, B. A.; van het Schip, A. D.; Koning, G. A.; Nijsen, J. F. W. Lanthanide-Loaded Liposomes for Multimodality Imaging and Therapy. *Cancer Biother. Radiol.* **2006**, *21*, 520–527.

14 Mitchell, D. G. *MRI Principles*; W. B. Saunders Company: Philadelphia, PA, 1999.

15 Koenig, S. H.; Keller, K. E. Theory of 1/*T*1 and 1/*T*2 NMRD Profiles of Solutions of Magnetic Nanoparticles. *Magn. Reson. Med.* **1995**, *34*, 227–233.

16 Morales, M. P.; Veintemillas-Verdaguer, S.; Montero, M. I.; Serna, C. J. Surface and Internal Spin Canting in $\gamma$-$Fe_2O_3$ Nanoparticles. *Chem. Mater.* **1999**, *11*, 3058–3064.

17 Cullity, B. D. *Introduction to Magnetic Materials*; Addison-Wesley publishing: Reading, MA, 1972.

18 (a) Yang, H.; Ito, F.; Hasegawa, D.; Ogawa, T.; Takahashi, M. Facile Large-Scale Synthesis of Monodisperse Fe Nanoparticles by Modest-Temperature Decomposition of Iron Carbonyl. *J. Appl. Phys.* **2007**, *101*, 09J112. (b) Vestal, C. R.; Zhang, Z. J. Synthesis of $CoCrFeO_4$ Nanoparticles Using Microemulsion Methods and Size-Dependent Studies of Their Magnetic Properties. *Chem. Mater.* **2002**, *14*, 3817–3822.

19 Lee, J.-H.; Huh, Y.-M.; Jun, Y.; Seo, J.-w.; Jang, J.-t.; Song, H.-T.; Kim, S. J.; Cho, E.-J.; Yoon, H.-G.; Suh, J.-S.; Cheon, J. Artificially Engineered Magnetic Nanoparticles for Ultra-Sensitive Molecular Imaging. *Nat. Med.* **2007**, *13*, 95–99.

20 Perez, J. M.; Josephson, Lee.; O'Loughlin, T.; Högemann, D.; Weissleder, R. Magnetic Relaxation Switches Capable of Sensing Molecular Interactions. *Nat. Biotechnol.* **2002**, *20*, 816–820.

21 Roch, A.; Gossuin, Y.; Muller, R. N.; Gillis, P. Superparamagnetic Colloid Suspensions: Water Magnetic Relaxation and Clustering. *J. Magn. Magn. Mater.* **2005**, *293*, 532–539.

22 Bitan, G.; Kirkitadse, M. D.; Lomakin, A.; Bollers, S. S.; Bennedek, G. B.; Teplow, D. B. Amyloid $\beta$-Protein (A$\beta$) Assembly: A$\beta$40 and A$\beta$42 Oligomerize Through Distinct Pathways. *Proc. Natl. Acad. Sci. U.S.A.* **2003**, *100*, 330–335.

23 Choi, J.-s.; Choi, H. J.; Jung, D. C.; Lee, J.-H.; Cheon, J. Nanoparticle Assisted Magnetic Resonance Imaging of the Early Reversible Stage of Amyloid $\beta$ Self-Assembly. *Chem. Commun.* **2008**, 2197–2199.

24 (a) Hermanson, G. T. *Bioconjugate Techniques; Academic Press*: New York, 1996. (b) Choi, J.-s.; Jun, Y.-w.; Yeon, S.-I.; Kim, H. C.; Shin, J.-S.; Cheon, J. Biocompatible Heterostructured Nanoparticles for Multimodal Biological Detection. *J. Am. Chem. Soc.* **2006**, *128*, 15982–15983.

25 Seidenfaden, R.; Krauter, A.; Schertzinger, F.; Gerardy-Schahn, R.; Hildebrandt, H. Polysialic Acid Directs Tumor Cell Growth by Controlling Heterophilic Neural Cell Adhesion Molecule Interactions. *Mol. Cell. Biol.* **2003**, *23*, 5908–5918.

26 Lee, J.-H.; Jun, Y.-w.; Yeon, S.-I.; Shin, J.-S.; Cheon, J. Dual-Mode Nanoparticle Probes for High-Performance Magnetic Resonance and Fluorescence Imaging of Neuroblastoma. *Angew. Chem., Int. Ed.* **2006**, *45*, 8160–8162.

27 Misselwitz, B. MR Contrast Agents in Lymph Node Imaging. *Eur. J. Radiol.* **2006**, *58*, 375–382.

28 Choi, J.-s.; Park, J. C.; Kim, M.-y.; Nah, H.; Woo, S.; Yun, S. Y.; Kim, K. M.; Cheon, G.; Chang, Y.; Yoo, J.; Cheon, J. A Hybrid Nanoparticle Probe for Dual-modality Positron Emission Tomography and Magnetic Resonance Imaging. *Angew. Chem., Int. Ed.* **2008**, *47*, 6259–6262.

29 Song, H.-T.; Choi, J.-s.; Huh, Y.-M.; Kim, S.; Jun, Y.-w.; Suh, J.-S.; Cheon, J. Surface Modulation of Magnetic Nanocrystals in the Development of Highly Efficient Magnetic Resonance Probes for Intracellular Labeling. *J. Am. Chem. Soc.* **2005**, *127*, 9992–9993.

30 Huh, Y.-M.; Lee, E.-S.; Lee, J.-H.; Jun, Y.-w.; Kim, P.-H.; Yun, C.-O.; Kim, J.-H.; Suh, J.-S.; Cheon, J. Hybrid Nanoparticles for Magnetic Resonance Imaging of Target-Specific Viral Gene Delivery. *Adv. Mater.* **2007**, *19*, 3109–3112.

31 Bulte, J. W. M.; Kraitchman, D. L. Monitoring Cell Therapy Using Iron Oxide MR Contrast Agents. *Curr. Pharma. Biotechnol.* **2004**, *5*, 567–584.

32 Hama, S.; Akita, H.; Ito, R.; Mizuguchi, H.; Hayakawa, T.; Harashima, H. Quantitative Comparison of Intracellular Trafficking and Nuclear Transcription Between Adenoviral and Lipoplex Systems. *Mol. Ther.* **2006**, *13*, 786–794.

33 Bergelson, J. M.; Cunningham, J. A.; Droguett, G.; KurtJones, E. A.; Krithivas, A.; Hong, J. S.; Horwitz, M. S.; Crowell, R. L.; Finberg, R. W. Isolation of a Common Receptor for Coxsackie B Viruses and Adenoviruses 2 and 5. *Science* **1997**, *275*, 1320–1323.

34 Pankhurst, Q. A.; Connolly, J.; Jones, S. K.; Dobson, J. Applications of Magnetic Nanoparticles in Biomedicine. *J. Phys. D: Appl. Phys.* **2003**, *36*, 167–181.